Polymer Chemistry

Self-Assembly of Highly Asymmetric, Poly(Ionic Liquid)-rich Diblock Copolymers and the Effects of Simple Structural Modification on Phase Behaviour

Journal:	*Polymer Chemistry*
Manuscript ID	PY-ART-10-2018-001414.R1
Article Type:	Paper
Date Submitted by the Author:	05-Dec-2018
Complete List of Authors:	May, Alyssa; Colorado State University , Chemistry Shi, Zhangxing; University of Colorado Boulder, Chemistry Wijayasekara, Dilanji; Colorado State University, Chemical and Biological Engineering Gin, Douglas; University of Colorado Boulder, Chemistry Bailey, Travis; Colorado State University, Chemical and Biological Engineering

SCHOLARONE™
Manuscripts

Polymer Chemistry

ARTICLE

Self-Assembly of Highly Asymmetric, Poly(Ionic Liquid)-rich Diblock Copolymers and the Effects of Simple Structural Modification on Phase Behaviour

Alyssa W. May,[a] Zhangxing Shi,[b] Dilanji B. Wijayasekara,[c] Douglas L. Gin,[b,d] and Travis S. Bailey[a,c,e],*

A series of thermally processable, phase separating diblock copolymers made via sequential ATRP of styrene and styrenic ionic liquid (IL) monomers with various alkyl imidazolium substituents were synthesized to cover a wide range of volume fractions, most notably those on the IL-rich side of the phase diagram. Small-angle X-ray scattering (SAXS) analysis was used to confirm melt-state (and glassy state) phase behavior in which all four classic equilibrium diblock copolymer morphologies – body-centered cubic spheres (S_{BCC}), hexagonally packed cylinders (Hex), lamellae (Lam), and notably, bicontinuous gyroid (Gyr) – were observed. These PS-PIL diblock copolymers were found to have a high degree of conformational asymmetry and/or electrostatic cohesion within the PIL block, highlighted by the shift of the Lam phase window with boundaries falling between $f_{PIL} = 0.31$ and 0.55. Variation of the alkyl group appeared to influence the strength of the Flory-like interaction parameter of the system, $\chi_{PS/PIL}$, such that simple substitution of methyl by n-butyl on the imidazolium IL substituent resulted in the emergence of the (notoriously segregation-sensitive) Gyr phase, superseding the persistent coexistence of Lam and Hex in the methyl-substituted imidazolium diblock copolymer phase diagram.

Introduction

Ionic liquids (ILs) have been a major focal point in many areas of chemistry and engineering due to their favourable properties and emerging capabilities. ILs are popular as solvents for green chemistry due to their near-zero vapor pressure and negligible flammability. Their high ionic conductivity, stability, and sorption selectivity for certain light gases also make them attractive for use in energy applications[1] (i.e., as electrolytes in batteries[2] and post-combustion gas separation membranes[3]). In circumstances where the mechanical properties of a polymer are more desirable, researchers have turned to polymerized ionic liquids (PILs), or polymers that incorporate the (typically) cationic portion of the IL as part of each polymeric repeat unit.[4,5] The counter-anion remains separate and weakly coordinated to the polymer backbone, which allows the material to maintain good ionic conductivity.

Due to the liquid-like nature of many PIL homopolymers of interest, the ability to tune the mechanical and other properties of PILs can be limited. One strategy to mitigate this problem has been to generate block copolymers (BCPs) containing a PIL block (PIL-BCPs). Taking advantage of the tunability of BCP morphologies and their associated long-range nanostructures gives PIL-BCPs the advantage of having one block dedicated to providing mechanical integrity while allowing the PIL block to retain many of the desirable qualities of the IL on which it is based.[1,6] To produce PILs, incorporating IL functional units into a polymer backbone has been a commonly used strategy in recent years.[1,4–6] Most often, these BCPs – which are frequently styrene-, acrylate-, vinyl-, or norbornene-based – contain a modified imidazolium-based IL component (typically with an alkyl substituent), but quaternized ammonium[7] and phosphonium salts have been reported as well.[1,4–6] Diblock copolymer (AB) architectures are typically the most widely synthesized; however, Matyjaszewski and co-workers recently reported several interesting BCP architectures including ABA or BCB triblock copolymers in which B is the charged PIL block.[8]

Generally, there have been three strategies employed to synthesize PIL-BCPs.[1,6] These include (1) the post-polymerization modification of reactive groups on an uncharged BCP with an IL moiety, (2) the growth of PIL blocks on an uncharged macroinitiator, and (3) the sequential copolymerization of non-ionic and IL monomers. A multitude of polymerization techniques[1,6] have been used to achieve this, including the earliest examples of PIL-BCPs synthesized

[a.] Department of Chemistry, Colorado State University, Fort Collins, CO 80523-1872, USA. E-mail: travis.bailey@colostate.edu

[b.] Department of Chemistry and Biochemistry, University of Colorado, Boulder, Colorado, 80309, USA.

[c.] Department of Chemical and Biological Engineering, Colorado State University, Fort Collins, CO 80523-1370, USA.

[d.] Department of Chemical and Biological Engineering, University of Colorado, Boulder, Colorado, 80309, USA

[e.] School of Advanced Materials Discovery, Colorado State University, Fort Collins, CO 80523, USA

via nitroxide-mediated polymerization (NMP),[7,9,10] reversible addition-fragmentation chain-transfer (RAFT) polymerization,[11,12] atom-transfer radical polymerization (ATRP),[8,13,14] ring-opening metathesis polymerization (ROMP),[15] and anionic polymerization,[1] among others.[16]

While the synthetic development of novel PIL-BCPs continues to be a major research focus, it is also crucial that the self-assembly thermodynamics of this relatively new class of materials are fully understood and characterized. For example, Mahanthappa and co-workers showed that the conductivity of various styrene/imidazolium-functionalized styrenic BCPs varied widely depending on morphology, long-range order, and preparation of the polymer film.[9] Additionally, for polymers intended as gas separation membranes, Drzal et al. and Nguyen et al. both showed that BCP morphology had a direct impact on the gas transport properties of the material.[17,18] Therefore, we have spent some time focusing on applying polymerization techniques to IL monomers that allow for precise control over block ratios and molecular weight, as a means to probe the comprehensive phase separation behaviour of various PIL-BCP systems. We previously published work elucidating the phase behaviour of a series of alkyl-imidazolium norbornene block copolymers synthesized via ROMP.[15,19] In fact, this was one of the earliest studies to show that imidazolium-based PIL-BCPs are capable of forming ordered nanostructures by phase separation in the neat melt. Some significant drawbacks to this norbornene system (i.e., the need for expensive ROMP catalysts, lengthy monomer synthesis, and poor mechanical properties due to the liquid-like[19] nature of this BCP) led to exploration of more convenient polymerization techniques and monomers.

More recently, our groups performed a preliminary study[14] investigating the morphology of several styrene/styrenic alkyl-imidazolium BCPs similar to those synthesized by He et al and Weber et al.[8,9] This class of materials has several advantages over the norbornene/ROMP system including (1) lower cost, (2) flexibility and ease of synthesis, (3) reduced metal contamination, (4) easier room-temperature handling and storage (solid powders vs. viscous liquids), and (5) thermal processability. While Mahanthappa and coworkers prepared a similar product by post-polymerization modification of a styrene/4-vinylbenzyl chloride-based BCP, our groups and the Matyjaszewski group showed that imidazolium-based PIL-BCPs can be made by direct ATRP of IL monomers and uncharged monomers in scalable quantities with excellent control and purity. Since then, we have set out to further explore the self-assembly behavior and expand the known phase diagram for the linear diblock copolymer architecture of this class of materials. We believe a detailed understanding of how the densely charged PIL block influences BCP phase behavior even in these simple systems will add to the foundation from which more complex phase behavior of PIL-BCPs can be investigated, such as higher-order, linear BCPs (ABA, ABC, ABAC, etc.),[20–23] small molecule-doped BCPs,[24] pom-pom BCPs,[25] or BCPs
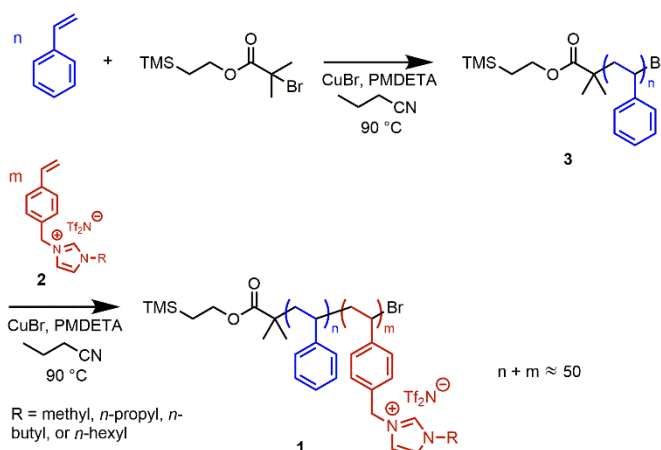
Scheme 1 Synthesis and structures of the PS-PIL BCPs made via sequential ATRP in this study.

incorporated into unusual matrices.[26] Thus, in contrast to the ROMP/norbornene monomer system studied initially where the focus was on PIL-BCPs with a majority volume fraction in the non-ionic block, we expand the phase diagram to the PIL-rich region ($f_{PIL} > 0.5$). Herein, we present the melt-state phase behavior of these alkyl-imidazolium-containing styrenic diblock BCPs made by sequential ATRP as function of (a) PIL block volume fraction and (b) different alkyl groups on the imidazolium of the PIL block.

Results and discussion

Synthesis and Characterization of PS-PIL BCPs

PS-PIL BCPs (1) were synthesized via the sequential ATRP procedures as described in our previous report; this is briefly outlined in Scheme 1.[14] In this two-step sequential copolymerization, polystyrene (3) of controlled molecular weight and low PDI was first synthesized as a macroinitiator for the second PIL block. The imidazolium-based PIL block was then formed upon addition of the appropriate amount and type of IL monomer (2). The BCPs synthesized were targeted to contain approximately 50 total repeat units while varying the relative volume fraction of the PIL block. The block composition ratio and molecular weight of each PS-PIL BCP (1) were confirmed by ^{1}H NMR analysis (see the Supporting Information).[14] The average degree of polymerization of the PS blocks were determined by end-group analysis using the TMS fragment of the initiator. The PS-PIL ratios for each BCP were calculated by integrating and comparing distinct ^{1}H NMR signals indicative of unique protons associated with the respective PS and PIL repeat units. The degree of polymerization of the each PIL block was then determined based on the calculated block composition ratios and PS degree of polymerization. Consequently, the number-average molecular weight (M_n) values for BCPs **1** could be calculated by multiplying the degree of polymerization of each block by the molecular weights (MWs) of the respective repeat units (see Table 1 and the Supporting Information).

Table 1 Morphological characteristics of PS-PIL BCPs **1a–t** at room temperature after thermal annealing

BCP	n	m	f_{PIL}[a]	M_n[b] (g mol^{-1})	d_{100}* (nm)	Morphology	Observed q^*/q_{100}[c]
R = methyl							
1a[d]	15	35	0.89	18600	16.6[e]	S_{LLP}	form scattering
1b[d]	20	30	0.85	16700	16.5[e]	S_{BCC}	√2, √4, √6, √8, √10, √12, √14, (√16)
1c[d]	25	25	0.79	14900	12.7	Hex (weakly ordered)	√1, (√3), √4, √7, (√9), (√12), (√13)
1d	30	18	0.70	12000	14.8	Hex (weakly ordered)	√1, √3, √4, √7, (√9), (√12), (√13)
1e	34	15	0.64	11000	16.7	Hex	√1, √3, √4, √7, (√9), √12, √13
1f	36	14	0.61	10800	16.7	Hex	√1, √3, √4, √7, (√9), √12, √13
1g	37	13	0.58	10400	15.5	Hex (weakly ordered)	√1, √3, √4, √7, (√9), (√12), (√13)
1h	40	12	0.55	10200	14.2	Lam (weakly ordered)	√1, √4, √9
					15.7	Hex (weakly ordered)	√1, √3, √4, (√7), (√9), (√12), (√13)
1i	34	10	0.54	8600	13.8	Lam	√1, √4, √9
					15.7	Hex	√1, √3, √4, (√7), (√9), √12, (√13)
1j	40	10	0.50	9200	13.0	Lam	√1, √4, √9
1k	40	9	0.48	8700	12.5	Lam	√1, √4, √9
1l	40	8	0.45	8300	12.3	Lam	√1, √4, √9
1m	45	5	0.31	7400	11.7	Lam	√1, √4, √9
					11.0	Hex	√1, √3, √4, (√7), (√9)
R = n-butyl							
1n[d]	15	35	0.90	20100	16.3[e]	S_{LLP}	form scattering
1o[d]	20	30	0.86	18000	15.6e	S_{BCC}	√2, √4, √6, (√8)
1p[d]	25	25	0.80	15900	11.3	Hex (weakly ordered)	√1, (√3), (√4), (√7), (√9),
1q	30	18	0.71	12800	14.5	Hex	√1, (√3), √4, √7, (√9),
1r	34	14	0.63	11100	15.0	Hex	√1, √3, √4, √7, √9, √12, √13
					15.3 (d$_{211}$)	Gyr	√6, √8, (√14), (√16), √20, √22, √24, (√26), (√30), (√32), (√38), (√40), √42, √46, (√48), (√50)
1s	40	9	0.49	9100	12.0	Lam	√1, √4, √9
1t	45	5	0.33	7600	12.1	Lam	√1, √4, (√9)
R = n-propyl							
1u	35	15	0.65	11500	15.4	Hex	√1, (√3), √4, √7, (√9), (√12), √13
1v	40	10	0.52	9500	13.2	Lam	√1, √4, √9
					14.0	Hex	√1, √3, √4, √7, (√9), (√12), (√13)
R = n-hexyl							
1w	20	30	0.86	18800	13.9	none	none observed
1x	25	25	0.80	16600	10.6	none	none observed

[a] f_{PIL} determined by $f_{PIL} = (M_{n,PIL}*\rho_{PIL}^{-1})/([M_{n,PIL}*\rho_{PIL}^{-1}]+[M_{n,PS}*\rho_{PS}^{-1}])$ where ρ_{PS} (0.969 g cm^{-3}) and ρ_{PIL} (1.06 g cm^{-3}, calculated from SAXS data of sample **1j**) are taken as nominal densities at 140 °C.[27] [b] Calculated based on n and m values obtained from ^{1}H NMR analysis and rounded down to nearest hundred g mol^{-1}.[14] [c] Permitted reflections for the specified morphology; those not observed are listed in parentheses. [d] Data integrated from previous work[14] [e] Calculated from d_{110} based on data from previous work.[14]

Overview of Phase Behavior

In a prior publication,[14] we reported the synthesis of several styrenic-imidazolium PS-PIL BCPs with varying R-group functionality (methyl, *n*-butyl, *n*-decyl) on the imidazolium block, and we included a preliminary assessment of the role of the R group on the ability of these BCPs to phase separate. Depending on the R-group, molar ratios of the IL block between 50–70% were observed to form spherical or cylindrical morphologies (methyl and *n*-butyl), or failed to phase separate (*n*-decyl). This revealed several intriguing characteristics about this polymer system. Specifically, R-group length significantly affected the ability of the PS-PIL BCPs to phase separate, and a much wider compositional range of samples would need to be produced to understand the phase behavior of these polymers. Due to the lack of observable phase separation with the series of *n*-decyl-substituted BCPs

previously studied,[14] the focus of our phase behavior investigation was narrowed to BCPs with R-groups containing up to six carbons, with an emphasis on those with terminal methyl and *n*-butyl groups.

Gel permeation chromatography (GPC) data of the PS macroinitiators (see Table S1 in the Supporting Information) in this study show fairly narrow PDIs (1.08 to 1.15), with no observable correlation between macroinitiator PDI and ability to phase separate. Modification to our GPC system according to previously reported methods[28] proved unsuccessful and PDIs of polymers **1a–1x** could not be calculated due to significant column interactions (see Supporting Information, section 6). Even though the PDIs of our final BCPs were unable to be measured, one of the many reasons ATRP was chosen as the synthetic method for this study is its ability to produce relatively narrow PDIs in polymers, PILs included.[8,13,14,28,29]

Small-angle X-ray scattering (SAXS) was used as the primary characterization method to describe the phase behaviour of various alkyl-substituted BCPs, polystyrene-*b*-poly(1-(4-vinylbenzyl)-3-alkyl (methyl, *n*-propyl, *n*-butyl, *n*-hexyl) imidazolium bis(trifluoromethanesulfonyl)imide) (PS-MePIL, PS-PrPIL, PS-BuPIL, PS-HxPIL). All samples were thermally annealed in the bulk under vacuum in the sample chamber of the SAXS instrument, with data collection typically taken every 50 °C, starting at room temperature. All samples were stepped to 175 °C, subjected to an annealing period between 30 min and 2 h, and then stepped back down to room temperature (see the full temperature-dependent SAXS data presented in the Supporting Information). A maximum temperature of 175 °C was chosen as a compromise between providing the polymer chains sufficient mobility to achieve at/near equilibrium phase behavior in a short amount of time (~15 min for most samples) and limiting the potential for thermal degradation (see figure S4.1-4.3 in the Supporting Information). This temperature is also well above the observed T_g's of the material (see Figure S5 in the Supporting Information) at ~80 °C for the PS block and ~32 °C for the MePIL block. Just under half of the samples showed ordered phases emerging at lower temperatures such as 100 °C or 125 °C, but all samples were annealed at 175 °C for consistency and efficiency.

Polymer phase behavior is best described by three fundamental parameters: (1) the volume fraction of one of the blocks (*f*), (2) the effective degree of segregation (χN), and (3) the conformational asymmetry (*ε*). Conformational asymmetry, while not shown explicitly in the phase diagram, accounts for the space-filling differences in the blocks of a BCP and routinely manifests itself as a shift in the phase boundaries of the phase diagram (such that symmetry around *f* = 0.5 is lost).[30,31] More recently, the parameter *Γ* was introduced to describe the strength of electrostatic cohesion between charged groups in a PIL block, and can also cause shifts (both horizontally and vertically) in the phase diagram.[32] In general, a BCP phase diagram maps out the specific equilibrium morphology at each composition and segregation strength for which the overall free energy of the BCP is minimized.[33] Generally, *f* would be calculated using bulk homopolymer
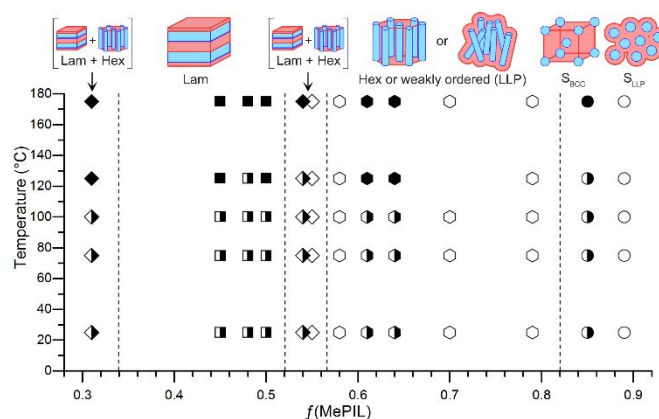

Fig. 1 Phase diagram for methyl-substituted PS-PIL BCPs 1a–m as a function of volume fraction of the PIL component. Open data points represent weakly ordered samples, filled data points represent highly ordered samples, and half-filled data points represent samples that ordered upon reaching an appropriate annealing temperature and remained ordered in that phase upon cooling.

densities to determine the relative ratio of block volumes, however, in this study the bulk homopolymer density of the largely unstudied alkyl-PIL blocks were unknown. However, it was possible to estimate the PIL block densities using characteristics of the SAXS diffraction data (see Lamellae section below for further explanation), allowing block compositions to be determined. χN is the product of χ, a Flory-like interaction parameter and N, the degree of polymerization. χ represents the free energy penalty (i.e. energy increase) associated with the interaction energy produced upon mixing of dissimilar repeat units.[33] While a typical phase diagram will present phase behavior data as χN versus composition (*f*), several factors that we, and others, have encountered with other PIL BCPs (e.g., an inability to disorder even low molecular weight PS-PIL BCPs at experimentally feasible temperatures) precluded simple determination of the value of $χ_{PS/PIL}$ for these systems of study.[9,15] Despite being unknown, the value of χ is largely considered to be independent of *f* for any A/B BCP pair. Additionally, as χ is inversely related to temperature, and all samples have a similar value of N (~50 repeat units) by synthetic design, reporting phase behaviour as a function of temperature (*T*) vs. composition (*f*) achieves a similar (although inverted) outcome as using a traditional χN vs. *f* plot.

In Figure 1, we report a summary of our study of phase behaviour results of the methyl-functionalized series of PS-MePIL BCPs, in which we were able to observe three out of the four classical diblock copolymer morphologies: Lam (data represented as square symbols in Figure 1), Hex (hexagon symbols), and S_{BCC} (circle symbols) organized on a body-centered cubic lattice. Samples that never achieved any high degree of order (or adopted a liquid-like packing rather than an organized lattice) are represented as open circle symbols; and samples that were initially weakly ordered but became well-ordered upon thermal annealing (and remained ordered during cooling) are represented as half-filled symbols. In the two areas on either side of the experimental phase diagram where the Gyr morphology would traditionally appear for a diblock copolymer, a persistent coexistence of Lam and Hex
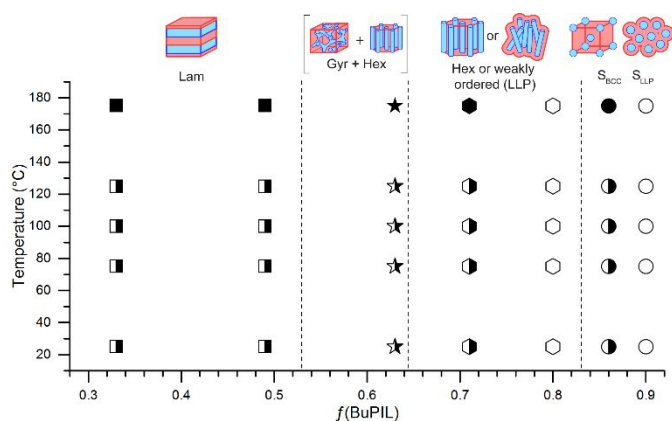
Fig. 2 Phase Diagram of phase separating, n-butyl-substituted PS-PIL BCPs **1n–t** with respect to volume fraction of the PIL component. Open data points represent weakly ordered samples, filled data points represent highly ordered samples, and half-filled data points represent samples that ordered upon reaching an appropriate annealing temperature and remained as such upon cooling. Data for samples with f_{BuPIL} greater than 0.8 are integrated from previous work.[14]
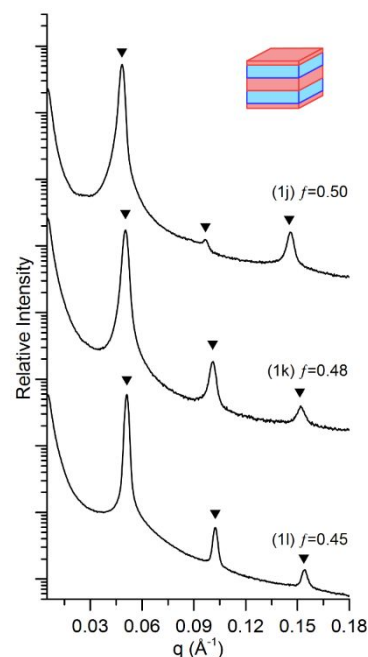

Fig. 3 Room temperature (25 °C) SAXS data collected post-annealing for lamellae-forming (Lam) PS-MePIL BCPs **1j–l**. Each sample was subjected to a two-hour annealing (*in vacuo*) at 175 °C. Solid inverted triangles represent the calculated values of allowed SAXS reflections (based on q*) for a Lam morphology, found at q/q^* ratios of √1, √4, and √9 (where q^*, the primary scattering wave vector, is q_{100}). Volume fractions were calculated from sample **1j**, where nearly complete suppression of the even-order reflection at $q/q^* = √4$ indicates equal volumes of either block ($f_{PIL} ≈ 0.5$)[9,15] and allowed for estimation of the bulk homopolymer density of MePIL.

(diamonds in Figure 1) was observed instead.[30,34–36] More compositionally asymmetric samples adopting a liquid-like packing of either cylinders or spheres provided the general location for the order-to-order (Hex to S_{BCC}) and order-to-disorder (S_{BCC} to S_{LLP}) phase boundaries on the high f_{PIL} side of the phase diagram. However, we were unable to observe any of the samples in this series in a completely disordered state.

Figure 2 shows the effect of modifying the R-group functionality of the dangling imidazolium unit (from methyl to *n*-butyl) on phase behaviour, and consequently, on decreasing the segregation strength between blocks. In a prior study, we were able to observe the Gyr morphology in coexistence with Hex in a series of metal-containing PIL-BCPs,[11] leading us to believe that indeed, the Gyr morphology should be observable in these imidazolium IL-containing BCPs, as well. However, its absence in the methyl-functionalized series was likely symptomatic of the high degree of segregation intrinsic to the system, notorious for thwarting Gyr formation.[37] However, by substitution of the methyl substituent with an *n*-butyl group, we found strong evidence for the emergence of a Gyr phase (in coexistence with Hex) in PS-PIL BCP **1r**. The full phase behaviour of the *n*-butyl series is discussed in detail below.

It is also of note that for all samples that formed ordered morphologies upon thermal annealing, no ordered-phase to ordered-phase transitions (OOTs) within any single sample were observed throughout the experimentally accessible range of temperatures examined (from room temperature to as high as 240 °C). That is, only one morphology (or persistent coexistence of morphologies) was observed for each individual sample. All morphologies developed through annealing at high temperature remained unchanged once cooled, even when annealed at lower temperatures just above the T_g of the PS block. In addition, the inability of these BCPs to disorder prior to thermal decomposition made it difficult to definitively classify any observed morphologies as true equilibrium phases, or directly determine the value of $\chi_{PS/PIL}$ from SAXS alone.[15,38–40] However, given the extremely large temperature window in

which they persisted once ordered, it is likely that most of the morphologies observed are in their equilibrium state; and for those that are in a persistent metastable state, the kinetics of

any OOT's are too prohibitively slow for the timescale of this study.

While analysing our earlier norbornene PIL-BCP system, we surmised that the inability to disorder most of these polymer samples without inducing decomposition provided strong evidence for an extremely high segregation strength (χN) between the blocks, despite the low degrees of polymerization (where N, or n+m ≤ 50). It is possible that χ is even higher in this study, as none of the BCPs studied showed any evidence of disordering, while two samples in the norbornene system either approached or even achieved disorder.

Below, we present a more detailed analysis of each morphology identified using SAXS data as a function of temperature for every PIL-BCP sample in this study. Each morphology-specific discussion refers to the methyl-substituted PIL-BCPs only, with a discussion of the *n*-butyl, *n*-propyl, and *n*-hexyl PIL-BCPs, respectively, following.

Lamellae

SAXS analysis of BCP samples **1j–l**, from 45 to 50% by volume of PIL, exhibited evidence of the Lam morphology, as shown in Figure 3. Upon thermal annealing, all of these

samples showed higher-ordered SAXS diffraction reflections at q/q^* ratios of √1, √4, and √9 (where q^* is the position of the primary scattering wave vector, q_{100}), consistent with the calculated allowed reflections[41] for this classic diblock copolymer morphology (solid inverted triangle symbols in Figure 3). These three samples, with approximate M_n values ranging from 8300 g mol^{-1} (**1l**) to 9300 g mol^{-1} (**1j**) were found to have small but steadily increasing domain spacings (d_{100} increasing from 12.3 to 13.0 nm, respectively) as is anticipated with a MW increase and the shift to higher PIL block content. Notably however, when compared with analogous but non-ionic Lam-forming diblock copolymers like polystyrene-*b*-poly(vinylpyridine), degrees of polymerization of nearly double (N ~ 95 − 105) are required to achieve similar domain spacing values.[42] This behaviour underscores the very extended nature of the ionic PIL block in the melt and its strong predilection for adopting a stretched chain conformation during self-assembly.

The near extinction of the even-order reflection $q/q^* = $ √4 in sample **1j** suggests nearly symmetrical block volumes, a phenomenon observed previously with our norbornene-based PIL-BCPs and with the *n*-hexyl-functionalized styrene-imidazolium BCPs studied by Mahanthappa and coworkers.[9,15] Using the bulk homopolymer density of polystyrene of 0.969 g cm^{-3} (at 140 °C)[43] and setting the relative volumes of the two blocks to 0.50, we were able to calculate an approximate density for the MePIL block of 1.06 g cm^{-3}. This value was then used in conjunction with experimentally determined M_n values of each block (calculated from ^{1}H NMR data) to estimate the volume fraction of PIL for each PIL-BCP in this series. Interestingly, the difference between samples **1j** and **1k**, in which the $q/q^* = $ √4 peak is suppressed, and clearly present, respectively, is only a single (on average) added MePIL repeat unit. Thus, even though suppression of the $q/q^* = $ √4 is not absolute in **1j**, our estimation of the PIL block density is believed to be reasonably accurate given the apparent sensitivity of the $q/q^* = $ √4 peak extinction to very small changes in BCP composition.

Hexagonally Packed Cylinders

In the region spanning $f_{PIL} = 0.58$ to 0.79, SAXS data of samples **1c–g** with M_n values ranging from 10400 to 14900 g mol^{-1} showed evidence of the hexagonally-packed cylinder (Hex) morphology with all samples exhibiting multiple higher order SAXS reflections at allowed q/q^* ratios of √1, √3, √4, √7, √9, √12, and √13 (shown as hollow inverted triangle symbols in Figure 4). This transition in phase behaviour in the PIL-rich region from a Lam to Hex phase just beyond $f_{PIL} = 0.5$ leads to the construction of a highly asymmetrical phase diagram. In the PS-rich region, however, we do not observe a Hex phase emerging until $f_{PIL} = 0.31$(see next section for discussion of these coexistence regions). One way to quantify the asymmetry is with the conformational symmetry ratio, ϵ, which describes the inequality in space-filling characteristics of each block, where an $\epsilon \neq 1$ indicates a conformationally asymmetric polymer. A significant shift in the phase boundaries here suggests that the ϵ value of this BCP is
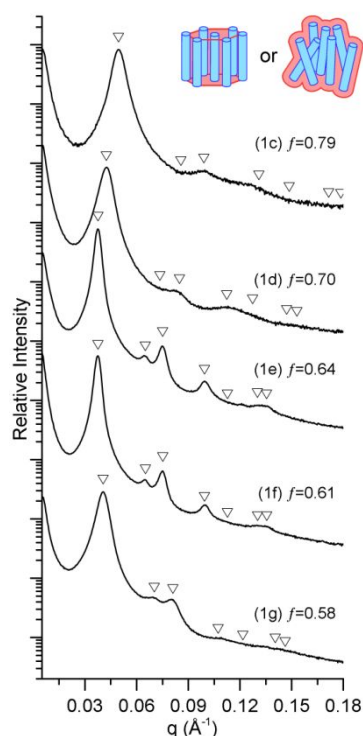

Fig. 4 Room temperature SAXS profiles (25 °C) collected post-anneal for hexagonally packed cylinder (Hex) forming PS-MePIL BCPs **1c–g**. Samples **1d–g** were subject to a two-hour annealing (*in vacuo*) at 175 °C, while sample **1c** was annealed for 30 min. Open inverted triangle symbols represent the calculated values of allowed SAXS reflections for a Hex morphology, at q/q^* ratios of √1, √3, √4, √7, √9, √12, and √13 (where $q^* = q_{100}$). Samples **1e** and **1f** exhibit a high degree of order (left cartoon above), while the rest, 1c, **1d**, and **1g** more closely match a liquid-like packing of cylinders (right cartoon above).

significant; however, we are unable to calculate its value without the statistical segment length (*b*) of each block, which to our knowledge, has not been determined for any styrenic imidazolium-based PIL.[30,35,39,44] We assume the shift in phase boundary occurs due to a much larger statistical segment length in the MePIL block, itself a product of an extended conformation of the main chain associated with both steric and electrostatic repulsion among the bulkier cationic imidazolium side groups.[39] When the PIL block occupies the majority of the volume, it encourages the interface between the PS and MePIL blocks to curve towards the PS domain, initiating a shift towards the PS cylinder phase at lower volume fractions of PIL than would otherwise be predicted for a conformationally symmetric polymer of $f_{PIL} > 0.5$.[30,35] This effect is reminiscent of phase diagrams of other highly asymmetric block copolymers with an $\epsilon > 2$, such as poly(ethylene oxide)-b-polyisoprene (PEO-PI)[44] and the "brush-like" diblock copolymer poly(1,2-octylene oxide)-*b*-poly(ethylene oxide) (POO-PEO).[34]

Alternatively or concurrently, electrostatic cohesion or Coulomb interaction strength (Γ) between charged repeat units on the PIL block could be contributing to the asymmetry of this phase diagram. Theoretical work by Olvera de la Cruz and coworkers[32] indicates that charged groups embedded into one block of a BCP can shift phase boundaries towards lower volume fractions of that charged block in the same way as
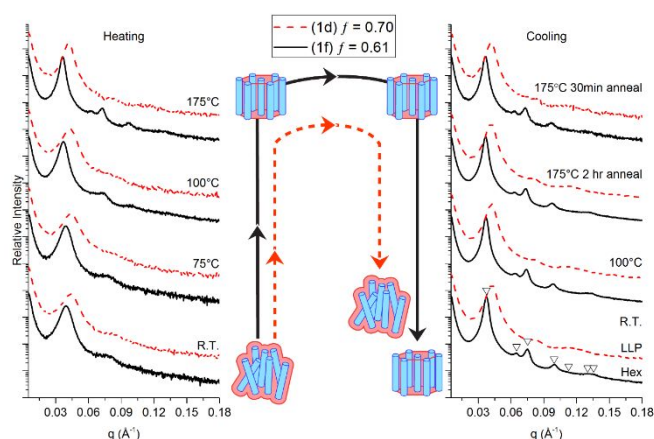
Fig. 5 Temperature-dependent SAXS profiles for cylinder-forming samples **1d** and **1f** illustrating the difference in scattering profiles for a sample that formed highly-ordered, periodic hexagonal nanostructure very rapidly (**1f**), and a sample that phase separated rapidly but remained weakly ordered even after extended thermal annealing (**1d**).

conformational asymmetry. Higher values of Γ encourage nanostructure formation in a charged BCP with values of χN and f_{PIL} that are low enough to cause disorder in an uncharged polymer. These phase diagrams are the most skewed at values of $\chi N \leq 20\sim30$. At higher values of χN, the order of the phase boundaries more closely resemble those of an uncharged BCP system, albeit still shifted towards lower f_{PIL}, much like the phase diagram we have presented here. Whether the observed shifts in phase boundaries in our system are due to large values of ϵ, Γ, or some combination thereof, there is still little doubt that the χN parameter of our PS-PIL system is very high.

In this region of the phase diagram, we observed samples (**1c**, **1d**, **1g**) that experienced some difficulty in forming a highly ordered hexagonal packing, instead exhibiting more of a liquid-like packing of cylinders, even after two full hours of annealing at 175 °C (Figure 5). In the norbornene-imidazolium system previously studied, this weakly ordered morphology was easily transformed into a Hex phase through thermal annealing.[15] Because there is nothing thermodynamically favourable about weakly ordered cylinders, we expect that the observed lack of periodicity in samples **1c**, **1d**, and **1g** partially stems from extremely slow ordering kinetics as a result restricted chain mobility. This occurs when minority component chains experience difficulty diffusing through the majority matrix due to presumably high values of χ.[45,46] Additionally, their location in regions of f_{PIL} close to the Hex/S or Hex/Lam phase boundaries, may also be influencing their driving force to exhibit a strong degree of order.[45]

Coexistence of Lamellae and Cylinders

Three samples, **1h**, **1i**, and **1m**, with compositions of 0.55, 0.54, and 0.31 f_{PIL} (and M_n values of 10300, 8700 and 7400 g mol^{-1}) respectively, exhibited coexistence of Lam and Hex phases that persisted throughout the annealing process. In addition to two distinct q^* values (where q^*, the primary scattering wave vector, is q_{100} for both Lam and Hex phases), all samples showed at least one uniquely identifiable higher-
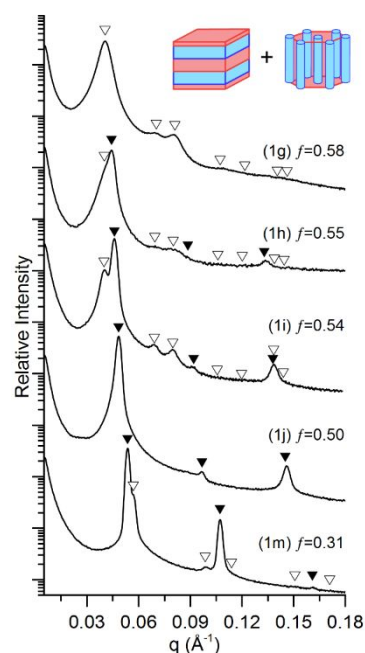

Fig. 6 Post-annealing SAXS data collected at room temperature (25 °C) for PS-MePIL BCPs 1h, 1i and 1m showing a persistent coexistence of the Lam and Hex phases. Samples 1g and 1j are included in this plot as BCPs that exhibit purely Hex and Lam morphologies, respectively, near the phase border. Samples 1h and 1i were subject to a 2-h annealing period (*in vacuo*) at 175 °C, while sample 1m was annealed for 8 h. Solid inverted triangle symbols represent the calculated positions of allowed SAXS reflections for a Lam morphology, at q/q^* ratios of √1, √4, and √9, and open inverted triangles represent the calculated positions of allowed SAXS reflections for a Hex morphology, at q/q^* ratios of √1, √3, √4, √7, √9, √12, and √13 (where $q^* = q_{100}$).

order SAXS reflection for each morphology. Specifically, scattering peaks at q/q^* ratios of √1, √4, and √9 for the Lam phases, and √1, √3, and √4 for the Hex phase (Figure 6) could be typically identified.

Another interesting effect of the conformational asymmetry of these PIL-BCPs appears to manifest itself in the relative positions of q_{HEX}^* and q_{LAM}^* in the two coexistence regions on either side of the Lam phase window. That is, while q_{HEX}^* is less than q_{LAM}^* for coexistence samples in the majority PIL region of the phase diagram, q_{HEX}^* is greater than q_{LAM}^* in the majority (non-ionic) PS region. The latter is consistent with the positioning of q_{HEX}^* and q_{LAM}^* in our previous study of norbornene based PIL BCPs, where the focus was limited to the investigation of BCPs with the non-ionic block comprising the majority component. It is not clear whether or not the inversion in q^* position between the two coexistence regions that span opposite sides of the lamellar window constitutes a general phenomenon in strongly segregated, conformationally asymmetric, and highly charged systems showing coexistent phases.

For all diblock copolymer morphologies except for Lam (which has both uniform domain thickness and constant mean curvature), there is a struggle between the need to have constant mean curvature to minimize interfacial tension between the blocks, and uniform domain thickness to maximize the entropic nature of chain stretching. This is known as packing frustration, because it is impossible to

satisfy both requirements completely when there is enough asymmetry to cause interfacial curvature.[47–49] Here, the bulky, space filling, and highly charged nature of the PIL block forces interfacial curvature towards the PS domains almost immediately after the PIL block becomes the majority component by volume ($f_{PIL} > 0.5$). Early adoption of curvature appears to be in response to a need to relieve packing frustration felt particularly by the relatively short and bulky PIL blocks. Even though the stretching entropy is slightly reduced when the PS domains are forced to stretch to fill to the centre of the relatively large cylindrical domains, gains are made in the relaxation of the PIL chains through their larger interfacial area per chain. The opposite is true when PS is the majority component; PS does not experience space constraints the way the PIL block does, so we observe the Lam phase over a wider range of f and smaller spacing between PIL cylinders on this side of the phase diagram.[50]

None of these three samples' SAXS patterns fit to any of the complex morphologies such as Gyr or the metastable hexagonally perforated lamellae. Given the apparent stability and small window of this coexistence between the Lam and Hex phases, it is probable that a complex morphology does not experimentally exist for this system. If this is the case, the most reasonable explanation is the ostensibly large χN values, even at high temperature. Polymers with low χN can adopt a Gyr morphology because the penalty for non-constant mean curvature is still more favourable relative to the entropic advantage of having a minority component with nearly uniform domain thickness.[27,48,49] For a diblock copolymer with larger χN values, morphologies in which the mean curvature must deviate significantly from a single constant value (characteristic of the Gyr phase) experience an increase in packing frustration that challenges the ability of these phases to remain experimentally stable.[50]

While conformational asymmetry has been shown to affect the locations of phase boundaries, conformationally asymmetric BCPs have been observed to adopt the Gyr morphology, even in the strongly segregated regime around $\chi N \approx 50$, so conformational asymmetry alone cannot account for the absence of this phase.[30,34,44] In fact, Cochran et al. showed that conformational asymmetry actually increased the width of the theoretical Gyr phase window at high segregations ($\chi N = 40, 80$), albeit the phase window was still extremely narrow.[51] Davidock et al. produced several examples of highly segregated polymers that formed the Gyr phase with χN values up to 120; however, these polymers were synthesized with anionic polymerization and therefore had very narrow PDI values.[37] Polydispersity has been shown to have significant effects on the location within the phase diagram of BCP morphologies[52] but also does not inherently discourage the formation of complex morphologies. Self-consistent field theory (SCFT) predicts the existence of a Gyr phase window for AB diblock copolymers (with PDIs of the A block between 1.0 and 2.0, and a monodisperse B block). But as polydispersity increases, that phase window narrows significantly. Above $\chi N \approx 20$, the Gyr phase window is virtually non-existent on the more asymmetrical side of the predicted

phase diagram for the most polydisperse model.[47] In 2005, Lynd and Hillmyer concluded that introducing polydispersity into a diblock copolymer melt causes it to relieve packing frustration much in the same way that conformational asymmetry does. That is, increased polydispersity in the minority component will encourage transitions to higher mean curvature (Lam → Hex), while increased polydispersity in the majority component will push the system to adopt decreased overall curvature (Hex → Lam). Indeed, they were able to observe the Gyr morphology in PEP-PLA (poly(ethylene-*alt*-propylene)-*b*-polylactide) BCPs in the weakly segregated regime ($\chi N \approx 10$ to 20) with PDIs of the respective blocks as large as 1.36 and 1.67 for one polymer.[53] Conversely, Bendejacq et al. studied a series of highly segregated ($\chi N > 50$) block copolymers and BCP/homopolymer blends with high PDIs that exhibited persistent coexistence of Lam and Hex phase in lieu of a Gyr phase.[54] Another consideration is the presence of charged groups along the polymer backbone. Balsara and coworkers studied a series of poly(styrenesulfonate-*b*-methylbutylene) (PSS-PMB) BCPs with nearly symmetric compositions but with varied N and sulfonation levels.[40] Interestingly, even with nearly 50% charged groups on the PSS block, they were able to observe the formation of the Gyr morphology and easily accessible disorder regions for polymers with N = 54 and χN values in the 10–20 range. For the polymers in this study with significantly larger N (and therefore larger χN), persistent coexistence regions without accessible disorder points were observed. Generally, increasing χN and the fraction of charged groups within the PSS domains of similar length PSS-PMB BCPs caused morphologies with increased curvature towards the non-charged block and increased the chance of observing coexistent phases instead of Gyr.

Although we suspect that the polydispersity of this series of PIL-BCPs is not as significant as those mentioned previously, the compounded effect of some polydispersity, high charge density and electrostatic cohesion, and substantial conformational asymmetry is playing a major role in the observed morphology in the region of extremely high χN that our methyl-functionalized PIL-BCPs appear to populate.
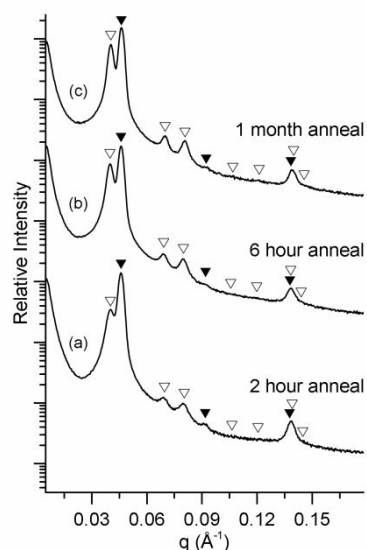
Fig. 7 Room-temperature SAXS data for sample **1i** showing persistent coexistence of Lam (solid inverted triangle symbols) and Hex (open inverted triangle symbols) after extended thermal annealing. Initially, the Lam phase dominates; but after 6 h of annealing at 175 °C, the Hex phase become more prevalent. After 1 month of thermal annealing under vacuum between 125 °C and 160 °C, a further shift toward the Hex phase is minimal, indicating that coexistence in this sample is persistent.

Even with a small amount of polydispersity within a polymer sample, self-fractionation during phase separation allows us to explain how a persistent coexistence of two very different morphologies lowers the free energy of the system enough to be preferable to the formation of Lam, Hex, Gyr phases or any metastable complex morphology alone. During the annealing process, more compositionally symmetric chains separate from more compositionally asymmetric chains to form Lam or Hex domains, respectively. SCFT models that allow distinct population distributions for each morphology have accounted for such behavior.[47] This phenomenon is only advantageous for a highly segregated sample; fractionation into discrete domains causes a significant reduction in system entropy, but this effect is negated by the overwhelming relief of packing frustration achieved through Lam and Hex phase coexistence.[47] This is a plausible explanation for the difference in primary scattering peak (q^*) resolution between samples **1h** and **1i**, which have nearly identical volume fractions. Sample **1h**, which is about 20% longer than **1i**, appears to have a compositional makeup (e.g., compositional polydispersity) or reduced mobility[45] that produces a diminished desire or ability to fractionate. This would lead to a smaller difference in domain spacing, less distinction between coexisting domains, and more weakly defined scattering patterns of both morphologies. Additionally, fractionation accounts for the structure factor extinction of the √4 Lam peak seen in sample **1i**, particularly in Figure 7, after extended annealing. The average volume fraction of PIL for **1i** is 0.54, but if the more symmetrical chains that separate to form the Lam domain were much closer to 0.50 then the √4 peak would disappear accordingly, as seen with sample **1j**.

Sample **1i** was subject to extended thermal annealing between 125 °C and 175 °C in a vacuum-sealed ampule and placed in an oil bath for a total of 1 month, as a means to investigate the stability and equilibrium nature of this phase coexistence (Figure 7). Within the first several hours of annealing, a shift in the prevalence for the Hex phase is apparent by the increase in intensity of q^*_{HEX} and the peaks at q/q^*_{HEX} = √3 and √4, coupled with a slight decrease in the q/q^*_{LAM} = √4 and √9 peaks shown by comparing Figures 7a and 7b. Beyond 6 h of annealing, the differences from 6 h to 1 month (Figures 7b and 7c) are very subtle, if not negligible, suggesting that at- or near-equilibrium phase behaviour is achieved within the first day of annealing, and that indeed, the coexistence phase is persistent.

Spheres

In the most compositionally asymmetric region of the phase diagram (f_{PIL} ≥ 0.85), two samples[14] showed SAXS patterns indicative of a sphere-based morphology. Upon thermal annealing, sample **1b** developed multiple higher-order SAXS reflections at q/q^* ratios (indicated as inverted triangle symbols with a strikethrough in Figure 8) of √2, √4, √6, etc., where q^* is the primary scattering wave vector, q_{100}, that are consistent with spheres arranged on a body-centred cubic lattice (S_{BCC}).[15] As is expected with S_{BCC}, q_{100} is absent due to the reflection conditions of the *Im3m* space group. The lattice constant ($a = d_{100}$) for samples **1a** and **1b** can be easily calculated from the first observed q value (q_{110}) giving values of 16.6 and 16.5 nm, respectively. The broad, form-factor scattering seen with sample 1a (and with 1b prior to annealing at 175 °C) is routinely observed for spherical micelles that persist with a liquid-like disordered packing (LLP), or S_{LLP}. The inability of spherical domains to order on a BCC lattice is typically due to compositional fluctuations near the ODT,
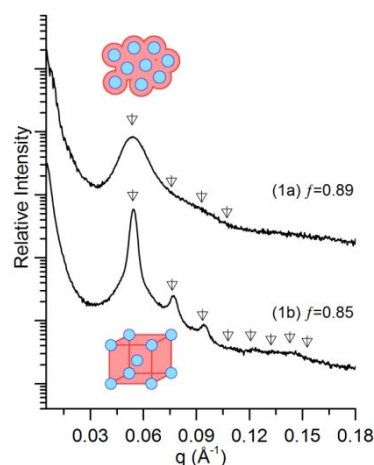

Fig 8. Post-annealing SAXS data at room temperature (25 °C) for sphere forming PS-MePIL BCPs **1a** and **1b.** Samples 1a and 1b were subject to a 30-min annealing period (in vacuo) at 175 °C. Open inverted triangles with a strikethrough represent the calculated allowed SAXS reflections for a sphere morphology arranged on a BCC lattice, at q/q^* ratios of √2, √4, √6, √8, √10, √12, √14 and √16 (where q^*, the primary scattering wave vector, is q_{100}). Sample 1a exhibits a more liquid-like packing of spheres (S_{LLP}), as opposed to the BCC lattice observed for **1b**.

sphere polydispersity, and limited chain mobility. The latter often a consequence of chain entanglements and slow chain diffusion kinetics.[15] As a result, S_{LLP} is often observed in samples with volume fractions that theoretically fall in the BCC range.[55,56] The persistence of liquid-like spherical domains in sample **1a** across the full experimental temperature range might imply that an f value of 0.89 PIL approaches the ODT but we are unable to pinpoint an actual disorder transition for this
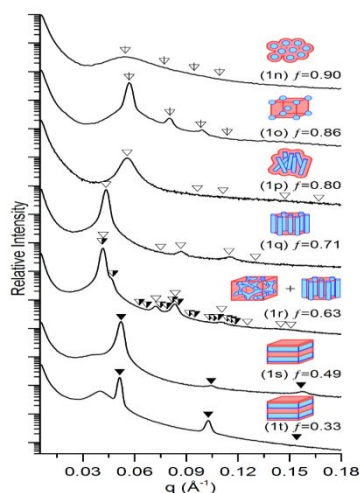

Fig. 9 Post-annealing, room temperature SAXS profiles for *n*-butyl-substituted PS-PIL BCPs **1n–t**. The allowed reflections for each morphology shown are represented as inverted triangles, including the possible emergence of the Gyr morphology (with expected peak locations denoted by half-filled triangle symbols above **1r** at q/q^* ratios of √6, √8, √14, √16, √20, etc. where q^*, the primary scattering wave vector, is q_{100}). The possible emergence of the Gyr morphology suggests a lower χ value n the *n*-butyl-substituted PS-PIL BCPs than that associated with the methyl-substituted PS-PIL BCPs.

system.

R-group Modification

In a preliminary study, we indirectly determined that R-group modification had a sizable impact on the interaction parameter χ between the PS and PIL blocks based on two observations; samples with *n*-butyl functionality but comparable block ratios had smaller d-spacings than their methyl counterparts, and the *n*-decyl-substituted blocks appeared to be miscible enough with the PS blocks to prevent phase separation altogether.[14] To investigate this effect further, we have prepared four additional *n*-butyl-functionalized BCPs (PS-BuPIL). The post-annealing room-temperature SAXS data for all seven samples are summarized in Figure 9. In this series we observe all four classic diblock copolymer morphologies; S_{BCC} (**1o**), Hex (**1q** and **1r**), Gyr (**1r**, in coexistence with Hex, represented as stars in Figure 2), and Lam (**1s** and **1t**), as well as two samples (**1n** and **1p**) that showed no higher order SAXS reflections but we suspect have adopted a liquid-packing of spheres and cylinders, respectively, based on their relative positions in the phase diagram (Figure 2).

We were unable to observe any structure factor extinction of the even-ordered reflections − such as the elimination of the $q/q^* = √4$ peak in sample **1j** − for the series of *n*-butyl-functionalized PIL BCPs, and therefore unable to estimate the

density of the BuPIL block based purely on SAXS evidence. To build a phase diagram using the volume fraction of the BuPIL block then, it was necessary to estimate the PIL block density using some known density values of similar block architectures, namely our density value of 1.06 g cm^{-3} for the MePIL block and Mahanthappa and coworkers' value of 1.096 g cm^{-3} for the HxPIL block.[9] It is reasonable to assume that our PIL block with *n*-butyl functionality would have a density falling between that of the methyl- and *n*-hexyl-functionalized polymers; and therefore, we estimate the block density of the BuPIL at 1.08 g cm^{-3}. This value was used to calculate the f_{PIL} values (listed in Table 1) for Figure 2.

Even though we were unable determine a quantitative value for χ, we believe we observe a significant enough shift with *n*-butyl R-group modification such that the Gyr morphology is able to emerge in coexistence with Hex in sample **1r** after extended thermal annealing (see the Supporting Information). This also affirms that χ (and consequently position within the phase diagram) is indeed tunable using the precisely controlled synthetic methods and selection of R group previously reported.[14] In this case, by adding a less polar group (i.e., *n*-butyl) to the end of the PIL repeat unit, we have achieved greater miscibility between the PS and PIL block. This effectively lowers the mixing penalty of the two blocks, relieving packing frustration within the system, and allowing the complex bicontinuous Gyr morphology to begin to form.[53]

Additionally, we prepared two *n*-propyl-functionalized samples, **1u** and **1v** (which exhibited phase behaviour similar to the PS-MePIL series) and two *n*-hexyl-functionalized samples, **1w** and **1x** (see Table 1 and section 3 of the Supporting Information for SAXS data) that showed phase separation but no higher-order SAXS reflections. Mahanthappa and co-workers investigated *n*-hexyl-functionalized polymers with identical structure that formed ordered nanostructures; however, they had significantly higher MW, and therefore much higher χN values.[9] Those samples were also on the PIL-lean side of the phase diagram (in contrast to the PIL-rich region on which we have focused). These differences make it difficult to glean any morphological insight about samples **1w** and **1x** from their work; but coupled with the observed shift in χN from the methyl to the *n*-butyl series discussed earlier, it is reasonable to infer that χN is lowered sufficiently in our *n*-hexyl series of polymers that these systems remain only weakly segregated and have difficulty establishing long-range periodic order.

Conclusions

We used SAXS data to show that a series of 13 methyl-, 2 *n*-propyl-, 7 *n*-butyl-, and 2 *n*-hexyl-functionalized PIL-BCPs synthesized via direct, sequential ATRP of styrene and styrenic imidazolium/Tf$_2$N IL monomers can form ordered, phase separated nanostructures that encompass the entirety of the classic diblock copolymer phase diagram. These ordered nanostructures, once formed through moderate annealing, were shown to remain well-ordered even upon cooling to

room temperature. The ability of these PIL-BCPs to remain ordered at ambient temperature, coupled with their easy handling, thermally processable nature, and intrinsic ionic conductivity,[9] suggests a potential future in solid-state polymer electrolyte membrane technologies.[1,57]

We were able to observe well-ordered samples forming sphere, cylinder, and Lam morphologies, and notably, one example of a Gyr phase in coexistence with the Hex phase. A Lam-forming sample exhibiting near structure factor extinction of the even-ordered SAXS reflection at a q/q^* ratio of √4 provided the means to estimate MePIL block density and consequently volume fraction (f) of the MePIL block. The compilation of these data was used to build two phase diagrams – one for the methyl and one for the n-butyl series – detailing their phase behaviour with respect to f_{PIL} and temperature. Temperature was used as a proxy for χN, due to a limited means of quantifying χ in this study. Regardless, we believe the χN values for the methyl series of PIL BCPs to be substantial based on an observed persistent coexistence of Lam and Hex phases in two separate samples where the Gyr morphology was anticipated. It was also noted that both phase diagrams showed a horizontal shift in phase behaviour due to some combination of electrostatic cohesion (Γ) within the highly charged PIL block and conformational asymmetry (ϵ) between the charged and uncharged blocks.

We also demonstrated the apparent ability to tune χ through modification of pendant alkyl groups on the imidazolium block by showing that the n-butyl-functionalized PIL-BCPs are capable of forming complex morphologies that are not present in the more highly segregated methyl-functionalized system. The bicontinuous network present in the Gyr morphology holds significant potential in many research areas – including conductive thin films,[58] transport applications,[59] solid-state batteries,[57] and organic photovoltaics[60] – where an ability to achieve charge transport in systems with domain continuity on the nanometer length scale has become so desirable.

Experimental

Materials and Methods

1-Bromopropane, 1-bromohexane, sodium hydride, imidazole, 1-methylimidazole, 1-butylimidazole, 4-vinylbenzyl chloride, 2-(trimethylsilyl)ethanol, α-bromoisobutyryl bromide, triethylamine, copper(I) bromide, butyronitrile, Dowex 50Wx4 ion-exchange resin, benzoyl peroxide, and N,N,N',N',N''-pentamethyldiethylenetriamine (PMDETA) were all purchased from the Sigma-Aldrich Co. and used as received. Styrene was purchased from the Sigma-Aldrich Co. and purified by passage through a column of neutral alumina to remove the added radical inhibitor. Lithium bis(trifluoromethylsulfonyl)amide (LiTf$_2$N) was purchased as Fluorad™ Lithium Trifluoromethane Sulfonimide from the 3M Company. All solvents were purchased from Sigma-Aldrich or Mallinckrodt, Inc. and purified/dehydrated via N$_2$-pressurized activated alumina columns, and de-gassed. The H$_2$O used for synthesis was

purified and deionized, with resistivity greater than 12 MΩ/cm. All polymerizations were carried out in a dry Ar atmosphere using standard Schlenk line techniques.

Instrumentation

^{1}H and ^{13}C NMR spectra were obtained using a Bruker 300 Ultrashield™ (300 MHz for ^{1}H) spectrometer. Chemical shifts are reported in ppm relative to residual non-deuterated solvent. HRMS (ES) analysis was performed by the Central Analytical Facility in the Dept. of Chemistry and Biochemistry at the University of Colorado Boulder. Gel permeation chromatography (GPC) was performed using a Viscotek GPC-Max chromatography system outfitted with three 7.5 x 340 mm Polypore™ (Polymer Laboratories) columns in series, a Viscotek differential refractive index (RI) detector, and an Alltech column oven (mobile phase: THF, 40 °C, 1 mL min^{-1} flow rate). Molecular weight data obtained on this GPC system were referenced to polystyrene molecular weight standards. SAXS data were collected using a Rigaku SMax3000 High Brilliance three-pinhole SAXS system outfitted with a MicroMax-007HFM rotating anode (Cu K$_\alpha$), a Confocal Max-Flux Optic, a Gabriel-type multi-wire area detector (1024 x 1024 pixel resolution), and a Linkam thermal stage. Differential scanning calorimetry (DSC) measurements were performed using a TA Instruments DSC 2500 with an RCS90 cooling system.

Small-Angle X-ray Scattering (SAXS) measurements

Copolymer samples were sandwiched between Kapton windows (0.06 mm thick × 10 mm diameter). Before collection of temperature-dependent SAXS data, the sample stage temperature was equilibrated for 5 min under vacuum, unless otherwise stated. Data were collected under vacuum (~100 mtorr) with exposure times ranging from 60 to 3600 s for all samples. SAXS data were azimuthally integrated from the 2D detector patterns and plotted as logarithmic intensity vs. the scattering wave vector, q, defined as $q = (4\pi/\lambda) \sin(2\theta_B/2)$, where $2\theta_B$ is the angle between the incident and scattered waves.

Synthesis of 1-propylimidazole

Synthesized as previously reported.[61] Characterization data matched those reported.[61]

Synthesis of 1-hexylimidazole

Synthesized as previously reported.[61] Characterization data matched those reported.[61]

Synthesis of 1-(4-vinylbenzyl)-3-alkylimidazolium bis(trifluoromethylsulfonyl)amide monomers (2)

These compounds were synthesized using the procedures previously reported.[14] The characterization data of monomers **2** matched those reported.[14,62,63]

Synthesis of 2-(Trimethylsilyl)ethyl 2-bromo-2-methylpropanoate (TMS-EBMP)

Synthesized as previously reported.[28] Characterization data matched those reported.[28]

Synthesis of polystyrene macro-initiators 3

These compounds were synthesized using the procedures previously reported.[14] In a typical procedure, the desired amount of purified styrene and PMDETA were added to a flame-dried Schlenk flask and degassed by three freeze-pump-thaw cycles. The flask was warmed to room temperature and back-filled with Ar, the desired amount of CuBr was then added. The resulting mixture was stirred at room temperature for 30 min, and TMS-EBMP was then injected. The flask was then stirred at 90 °C for 22 h. The contents of the flask were cooled to room temperature, dissolved in acetone, stirred with Dowex 50Wx4 ion-exchange resin for 30 min, and filtered through a short plug of neutral alumina. The resulting solution was then concentrated, diluted with Et_2O, precipitated by adding into MeOH, and filtered to give the desired PS macro-initiator **3** as a white solid. The *DP* and M_n values of BCPs **3** were calculated based on the ^{1}H NMR end-group analysis (see the Supporting Information).

Synthesis of PS-PIL BCPs 1

These compounds were synthesized using the procedures previously reported.[14] In a typical procedure, the appropriate amount of the desired imidazolium monomer **2**, PMDETA, and butyronitrile were added to a flame-dried Schlenk flask and degassed by three freeze-pump-thaw cycles. The flask was warmed to room temperature and back-filled with Ar, the appropriate amount of CuBr was then added. The resulting mixture was then stirred at room temperature for 30 min, and the appropriate amount of the desired PS macro-initiator **3** was added. The flask was then stirred at 90 °C for 24 h. The contents of the flask were cooled to room temperature, diluted with acetone, stirred with Dowex 50Wx4 ion-exchange resin for 15 min, and then filtered through a short plug of neutral alumina. The resulting solution was then concentrated, diluted with acetone, precipitated by adding into a MeOH/H_2O (3/1 (v/v)) mixture, and filtered. The resulting precipitate was then dissolved in acetone, re-precipitated by adding into hexanes, and filtered to give the desired BCP **1** as a white solid. The synthesis of **1j** is shown below as a representative example. The block compositions and M_n values of PS-PIL BCPs **1** were calculated based on the ^{1}H NMR analysis (see the Supporting Information).

Example: Synthesis of PS-PIL BCP 1j

1-(4-Vinylbenzyl)-3-methylimidazolium bis(trifluoromethylsulfonyl)amide (303 mg, 0.632 mmol), PMDETA (31.3 mg, 0.181 mmol), and butyronitrile (1.70 mL) were added to a flame-dried Schlenk flask and degassed by three freeze-pump-thaw cycles. The flask was warmed to room temperature and back-filled with Ar, CuBr (25.9 mg, 0.181

mmol) was added. The resulting mixture was stirred at room temperature for 30 min, and macroinitiator **3** (n = 40, 200 mg, 0.0451 mmol) was added. The flask was then stirred at 90 °C for 24 h. The resulting reaction mixture was purified as described in the general procedure above to give **1j** as a white solid (yield: 0.342 g, 82%). Block repeat unit molar ratio = 4:1 (PS:PIL); block length composition = 40-*b*-10 (PS-*b*-PIL); M_n = 9,227 $\cong$ 9200 g/mol (calculated based on ^{1}H NMR analysis; see the Supporting Information for details).

Conflicts of interest

There are no conflicts to declare.

Acknowledgements

References

1   K. M. Meek and Y. A. Elabd, *J. Mater. Chem. A*, 2015, **3**, 24568–24568.

2   I. Osada, H. de Vries, B. Scrosati and S. Passerini, *Angew. Chemie Int. Ed.*, 2016, **55**, 500–513.

3   D. B. Wijayasekara, M. G. Cowan, J. T. Lewis, D. L. Gin, R. D. Noble and T. S. Bailey, *J. Memb. Sci.*, 2016, **511**, 170–179.

4   N. Nishimura and H. Ohno, *Polymer*, 2014, **55**, 3289–3297.

5   D. Mecerreyes, *Prog. Polym. Sci.*, 2011, **36**, 1629–1648.

6   J. Yuan, D. Mecerreyes and M. Antonietti, *Prog. Polym. Sci.*, 2013, **38**, 1009–1036.

7   G. Sudre, S. Inceoglu, P. Cotanda and N. P. Balsara, *Macromolecules*, 2013, **46**, 1519–1527.

8   H. He, D. Luebke, H. Nulwala and K. Matyjaszewski, *Macromolecules*, 2014, **47**, 6601–6609.

9   R. L. Weber, Y. Ye, A. L. Schmitt, S. M. Banik, Y. A. Elabd and M. K. Mahanthappa, *Macromolecules*, 2011, **44**, 5727–5735.

10   C. M. Stancik, A. R. Lavoie, J. Schütz, P. A. Achurra, P. Lindner, A. P. Gast and R. M. Waymouth, *Langmuir*, 2004, **20**, 596–605.

11   Z. Shi, A. W. May, Y. Kohno, T. S. Bailey and D. L. Gin, *J. Polym. Sci. Part A Polym. Chem.*, 2017, **55**, 2961–2965.

12   K. Vijayakrishna, S. K. Jewrajka, A. Ruiz, R. Marcilla, J. A. Pomposo, D. Mecerreyes, D. Taton and Y. Gnanou, *Macromolecules*, 2008, **41**, 6299–6308.

13   N. A. Agudelo, A. M. Elsen, H. He, B. L. López and K. Matyjaszewski, *J. Polym. Sci. Part A Polym. Chem.*, 2015, **53**, 228–238.

14   Z. Shi, B. S. Newell, T. S. Bailey and D. L. Gin, *Polymer*, 2014, **55**, 6664–6671.

15   V. F. Scalfani, E. F. Wiesenauer, J. R. Ekblad, J. P. Edwards, D. L. Gin and T. S. Bailey, *Macromolecules*, 2012, **45**, 4262–4276.

16   C. Detrembleur, A. Debuigne, M. Hurtgen, C. J. er, J. Pinaud, M. F. eva evre, P. Coupillaud, J. Vignolle and D. Taton, 2011, **44**, 6397–6404.

17   P. L. Drzal, A. F. Halasa and P. Kofinas, *Polymer*, 2000, **41**, 4671–4677.

18   P. T. Nguyen, E. F. Wiesenauer, D. L. Gin and R. D. Noble, *J. Memb. Sci.*, 2013, **430**, 312–320.

19   E. F. Wiesenauer, J. P. Edwards, V. F. Scalfani, T. S. Bailey and D. L. Gin, *Macromolecules*, 2011, **44**, 5075–5078.

20   T. S. Bailey, C. M. Hardy, T. H. Epps and F. S. Bates, *Macromolecules*, 2002, **35**, 7007–7017.

21   T. H. Epps, E. W. Cochran, T. S. Bailey, R. S. Waletzko, C. M. Hardy and F. S. Bates, *Macromolecules*, 2004, **37**, 8325–8341.

22   E. F. Wiesenauer, P. T. Nguyen, B. S. Newell, T. S. Bailey, R. D. Noble and D. L. Gin, *Soft Matter*, 2013, **9**, 7923–7927.

23   S. Lee, M. J. Bluemle and F. S. Bates, *Science*, 2010, **330**, 349–353.

24   T. H. Epps, T. S. Bailey, R. Waletzko and F. S. Bates, *Macromolecules*, 2003, **36**, 2873–2881.

25   D. B. Wijayasekara, T. Huang, J. M. Richardson, D. M. Knauss and T. S. Bailey, *Macromolecules*, 2016, **49**, 595–608.

26   W. Fan, L. Wang and S. Zheng, *Macromolecules*, 2009, **42**, 327–336.

27   D. A. Hajduk, P. E. Harper, S. M. Gruner, C. C. Honeker, G. Kim, E. L. Thomas and L. J. Fetters, *Macromolecules*, 1994, **27**, 4063–4075.

28   H. He, M. Zhong, B. Adzima, D. Luebke, H. Nulwala and K. Matyjaszewski, *J. Am. Chem. Soc.*, 2013, **135**, 4227–4230.

29   J. Oh, J. Kuk, T. Lee, J. Ye, H.-J. Paik, H. W. Lee and T. Chang, *ACS Macro Lett.*, 2017, **6**, 758–761.

30   M. W. Matsen and F. S. Bates, *J. Polym. Sci. Part B Polym. Phys.*, 1997, **35**, 945–952.

31   D. A. Hajduk, H. Takenouchi, M. A. Hillmyer, F. S. Bates, M. E. Vigild and K. Almdal, *Macromolecules*, 1997, **30**, 3788–3795.

32   C. E. Sing, J. W. Zwanikken and M. Olvera De La Cruz, *Nat. Mater.*, 2014, **13**, 694–698.

33   F. S. Bates, *Science*, 1991, **251**, 898–905.

34   I. W. Hamley, B. M. D. O'Driscoll, G. Lotze, C. Moulton, J. Allgaier and H. Frielinghaus, *Macromol. Rapid Commun.*, 2009, **30**, 2141–2146.

35   F. S. Bates, M. F. Schulz, A. K. Khandpur, S. Förster, J. H. Rosedale, K. Almdal and K. Mortensen, *Faraday Discuss.*, 1994, **98**, 7–18.

36   F. S. Bates and G. H. Fredrickson, *Phys. Today*, 1999, **52**, 32.

37   D. A. Davidock, M. A. Hillmyer and T. P. Lodge, *Macromolecules*, 2003, **36**, 4682–4685.

38   D. A. Hajduk, S. M. Gruner, P. Rangarajan, R. A. Register, L. J. Fetters, C. Honeker, R. J. Albalak and E. L. Thomas, *Macromolecules*, 1994, **27**, 490–501.

39   J. H. Chu, P. Rangarajan, J. L. Adams and R. A. Register, *Polymer*, 1995, **36**, 1569–1575.

40   M. J. Park and N. P. Balsara, *Macromolecules*, 2008, **41**, 3678–3687.

41   S. Förster, A. Timmann, M. Konrad, C. Schellbach, A. Meyer, S. S. Funari, P. Mulvaney and R. Knott, *J. Phys. Chem. B*, 2005, **109**, 1347–1360.

42   Y. Matsushita, K. Mori, R. Saguchi, Y. Nakao, I. Noda and M. Nagasawaid, *Macromolecules*, 1990, **23**, 4313–4316.

43   L. J. Fetters, D. J. Lohse, D. Richter, T. A. Witten and A. Zirkel, *Macromolecules*, 1994, **27**, 4639–4647.

44   G. Floudas, B. Vazaiou, F. Schipper, R. Ulrich, U. Wiesner, H. Iatrou and N. Hadjichristidis, *Macromolecules*, 2001, **34**, 2947–2957.

45   P. M. Lipic, F. S. Bates and M. W. Matsen, *J. Polym. Sci. Part B Polym. Phys.*, 1999, **37**, 2229–2238.

46   T. P. Lodge and M. C. Dalvi, *Phys. Rev. Lett.*, 1995, **75**, 657–660.

47   M. W. Matsen, *Phys. Rev. Lett.*, 2007, **99**, 148304.

48   M. W. Matsen and F. S. Bates, *Macromolecules*, 1996, **29**, 7641–7644.

49   M. W. Matsen and F. S. Bates, *J. Chem. Phys.*, 1997, **106**, 2436–2448.

50   M. W. Matsen, *J. Phys. Condens. Matter*, 2002, **14**, R21–R47.

51   E. W. Cochran, C. J. Garcia-Cervera and G. H. Fredrickson, *Macromolecules*, 2006, **39**, 2449–2451.

52   J. M. Widin, M. Kim, A. K. Schmitt, E. Han, P. Gopalan and M. K. Mahanthappa, *Macromolecules*, 2013, **46**, 4472–4480.

53   N. A. Lynd and M. A. Hillmyer, *Macromolecules*, 2005, **38**, 8803–8810.

54   D. Bendejacq, V. Ponsinet, M. Joanicot, Y.-L. Loo and R. A. Register, *Macromolecules*, 2002, **35**, 6645–6649.

55   C. Guo and T. S. Bailey, *Soft Matter*, 2010, **6**, 4807–4818.

56   D. J. Kinning and E. L. Thomas, *Macromolecules*, 1984, **17**, 1712–1718.

57   S. Zekoll, C. Marriner-Edwards, A. K. O. Hekselman, J. Kasemchainan, C. Kuss, D. E. J. Armstrong, D. Cai, R. J. Wallace, F. H. Richter, J. H. J. Thijssen and P. G. Bruce, *Energy Environ. Sci.*, 2018, **11**, 185–201.

58   I. H. Ryu, Y. J. Kim, Y. S. Jung, J. S. Lim, C. A. Ross and J. G. Son, *ACS Appl. Mater. Interfaces*, 2017, **9**, 17427–17434.

59   L. Li, L. Schulte, L. D. Clausen, K. M. Hansen, G. E. Jonsson and S. Ndoni, *ACS Nano*, 2011, **5**, 7754–7766.

60   E. J. W. Crossland, M. Nedelcu, C. Ducati, S. Ludwigs, M. A. Hillmyer, U. Steiner and H. J. Snaith, *Nano Lett.*, 2009, **9**, 2813–2819.

61   C. J. Serpell, J. Cookson, A. L. Thompson, C. M. Brown and P. D. Beer, *Dalt. Trans.*, 2013, **42**, 1385–1393.

62   J. E. Bara, E. S. Hatakeyama, D. L. Gin and R. D. Noble, *Polym. Adv. Technol.*, 2008, **19**, 1415–1420.

63   J. E. Bara, S. Lessmann, C. J. Gabriel, E. S. Hatakeyama, R. D. Noble and D. L. Gin, *Ind. Eng. Chem. Res.*, 2007, **46**, 5397–5404.

for table of contents use only:
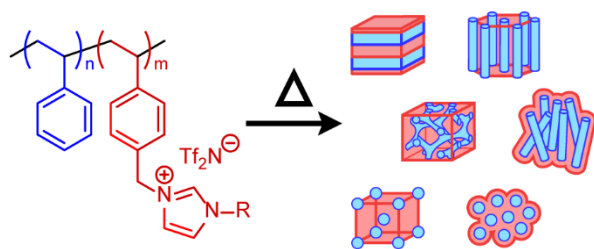
Self-Assembly of Highly Asymmetric, Poly(Ionic Liquid)-rich Diblock Copolymers and the Effects of Simple Structural Modification on Phase Behaviour

Alyssa W. May, Zhangxing Shi, Dilanji B. Wijayasekara, Douglas L. Gin, Travis S. Bailey

A series of ATRP-synthesized poly(IL) diblock copolymers exhibit morphological phase behavior with shifted phase boundaries and alkyl substituent dependent segregation.